Supporting Information

Surfactant-Free Vapor-Phase Synthesis of Single-crystalline Gold Nanoplates for Optimally Bioactive Surfaces

Youngdong Yoo,[†,&,‡] Hyoban Lee,[†,‡] Hyunsoo Lee,[||,§] Miyeon Lee,[†] Siyeong Yang,[†] Ahreum Hwang,[†,#] Si-in Kim,[†] Jeong Young Park,[||,§] Jaebum Choo,[+] Taejoon Kang,[#,¶,Δ] and Bongsoo Kim*[†]*

[†]*Department of Chemistry, KAIST, Daejeon 34141, Korea*

[&]*Department of Chemistry, University of Minnesota, Minneapolis MN 55455, USA*

[||]*Center for Nanomaterials and Chemical Reactions, IBS, Daejeon 34141, Korea*

[§]*Graduate School of EEWS, KAIST, Daejeon 34141, Korea*

[#]*Hazards Monitoring Bionano Research Center, KRIBB, Daejeon 34141, Korea*

[+]*Department of Bionano Engineering, Hanyang University, Ansan 15588, Korea*

[¶]*BioNano Health Guard Research Center, KRIBB, Daejeon 34141, Korea*

[Δ]*Department of Nanobiotechnology, KRIBB School of Biotechnology, UST, Daejeon 34113, Korea*

[*]To whom correspondence should be addressed.

E-mail: bongsoo@kaist.ac.kr (B.K.)

E-mail: kangtaejoon@kribb.re.kr (T.K.)

[‡]These authors contributed equally to this work.

1. Thin and small Au nanoplates grown on r-cut sapphire substrate

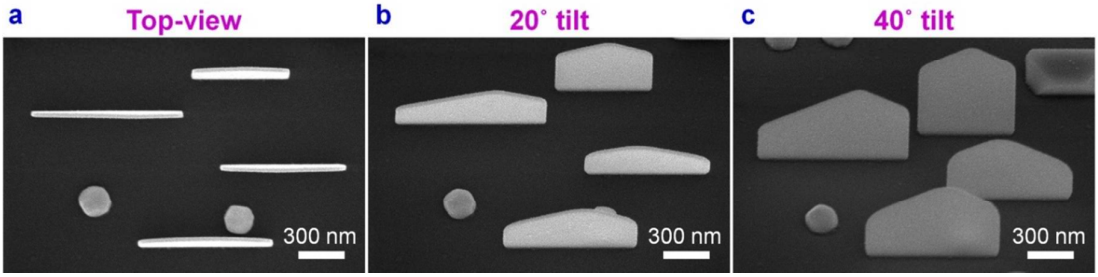

Figure S1. (a) Top-view, (b) 20˚ tilted-view, and (c) 40˚ tilted-view SEM images of small Au nanoplates grown on *r*-cut sapphire substrates.

2. Magnified AFM topographic image of Au nanoplate

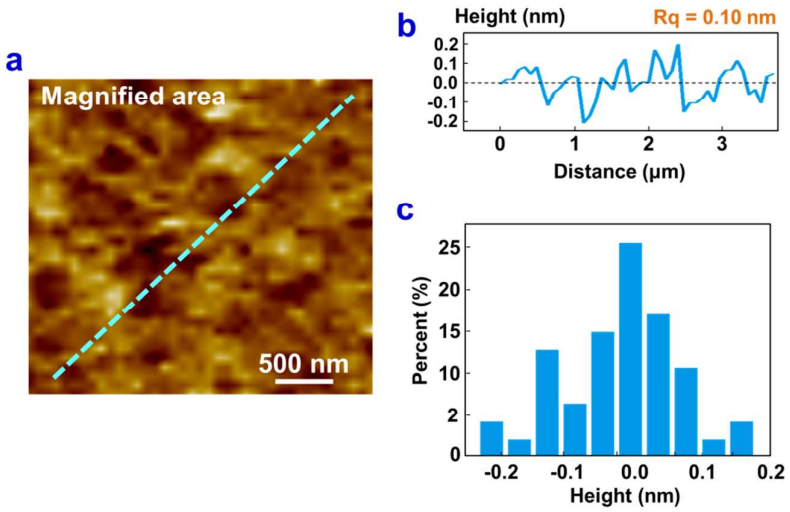

Figure S2. (a) Magnified AFM topographic image of Au nanoplate in Figure 2a. The scale is 3 μm × 3 μm. (b) Sectional view along a dotted cyan line in (a). The surface-height variation is between -0.2 nm and 0.2 nm with 0.10 nm of R_q. (c) Surface height distribution of (b).

3. Epitaxial relationship at the interface between Au seed NP and *m*-cut sapphire substrate

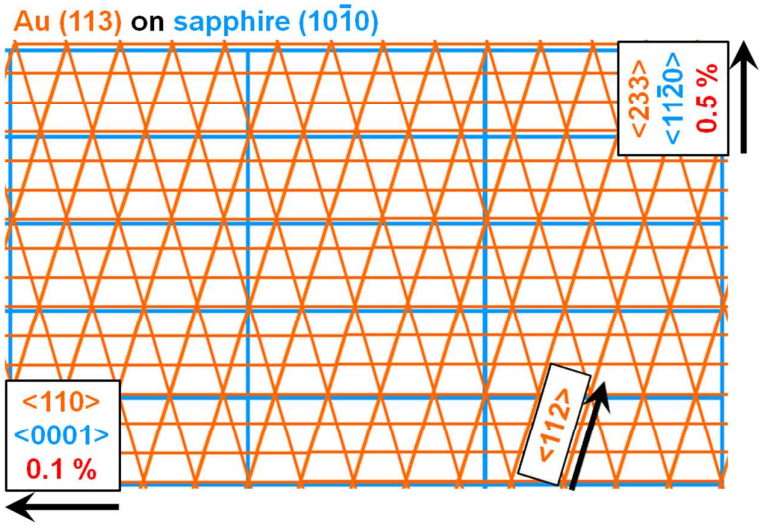

Figure S3. Schematic illustration of atomic planes at the epitaxial interface between Au (113) and sapphire (10$\bar{1}$0) planes. 9 layers of Au and 2 layers of sapphire have 0.1% domain-matched misfit along Au <110>//sapphire <0001> direction. The lattice spacing of the Au (110) plane is 1.44 Å and that of the sapphire (0001) plane is 6.49 Å.

4. Selective synthesis of Au nanostructures by deposition flux

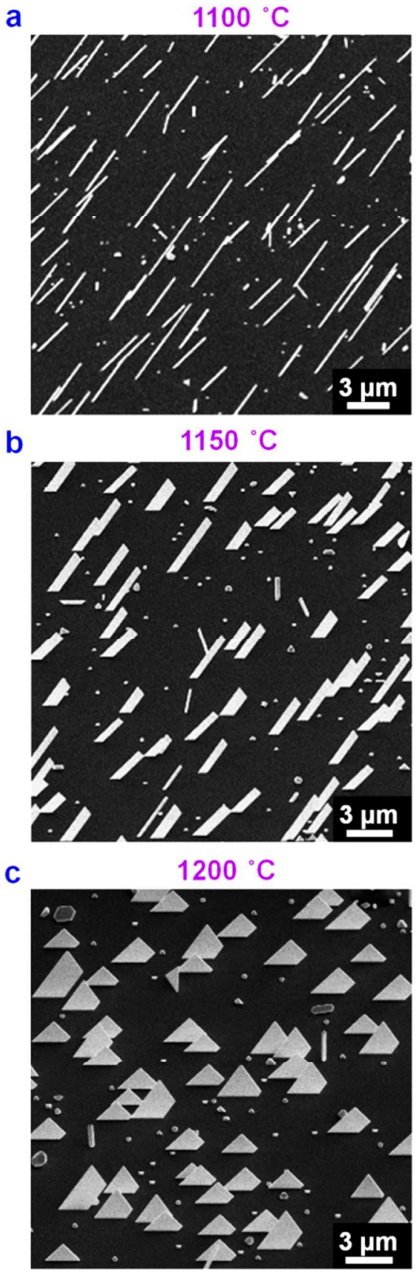

Figure S4. 45˚ tilted-view SEM images of (a) Au NWs, (b) nanobelts, and (c) nanoplates grown at a precursor temperature of 1100 ˚C, 1150 ˚C, 1200 ˚C, respectively. The temperature of *m*-cut sapphire substrates were maintained at 1000 ˚C for all experiments.

5. Synthesis of horizontal Au NWs in very high deposition flux condition

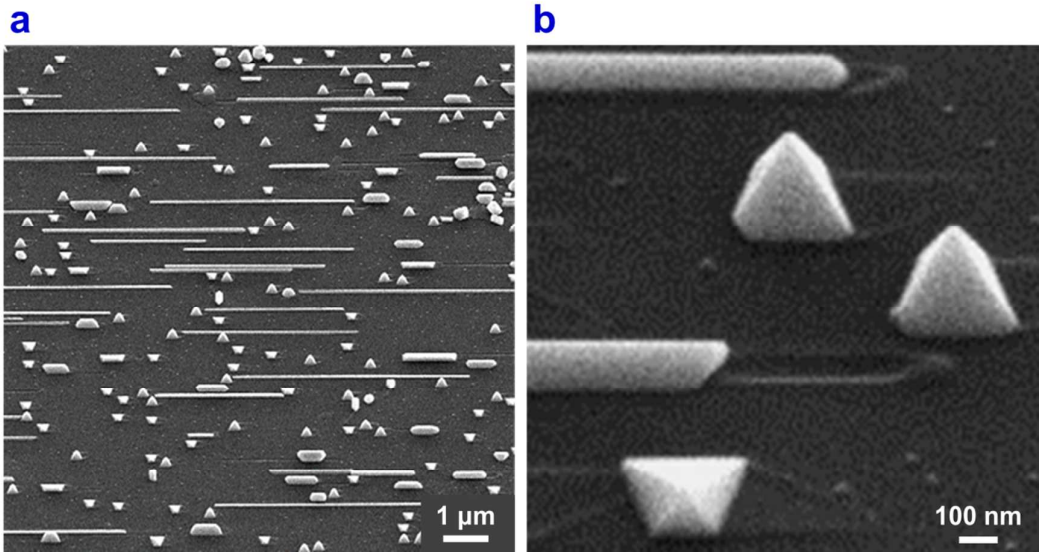

Figure S5. (a) Top-view and (b) Magnified and 45˚ tilted-view SEM images of horizontal Au NWs on *m*-cut sapphire substrate. Au power was used as a precursor instead of Au lump to increase the deposition flux of Au atoms. The precursor temperature was 1200 ˚C.

6. Au NPs on a nanoplate structure through the biotin-avidin interaction

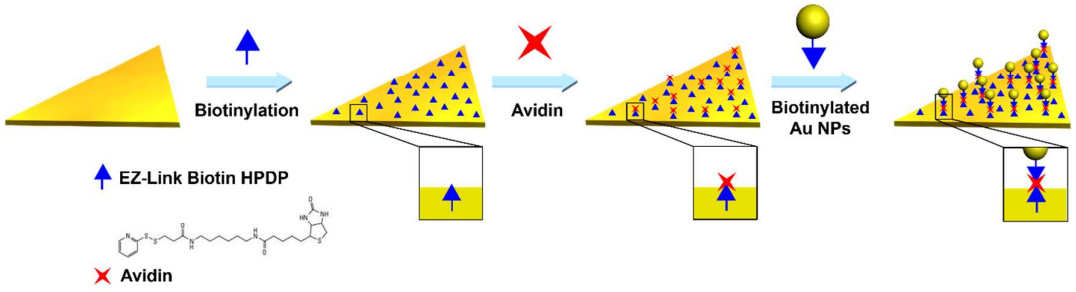

Figure S6. Schematic illustration of the construction process of Au NPs on a nanoplate structure through the biotin-avidin interaction.

7. Full SERS spectra corresponding Figure 6f

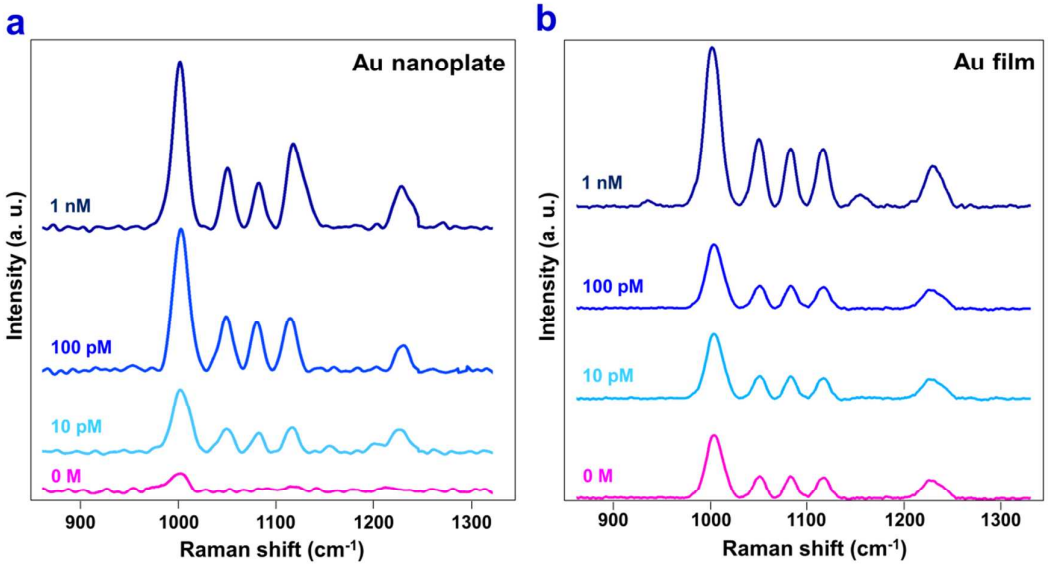

Figure S7. SERS spectra obtained from (a) Au NPs on a nanoplate structures and (b) Au NPs on a film structures with various avidin concentrations (0 M, 10 pM, 100 pM, and 1 nM). The ultraflat Au nanoplate-based SERS sensor has a detection limit of 10 pM, whereas the rough Au film-based SERS sensor has a detection limit of 1 nM.

8. SEM images of Au NPs on Au nanoplate and Au film

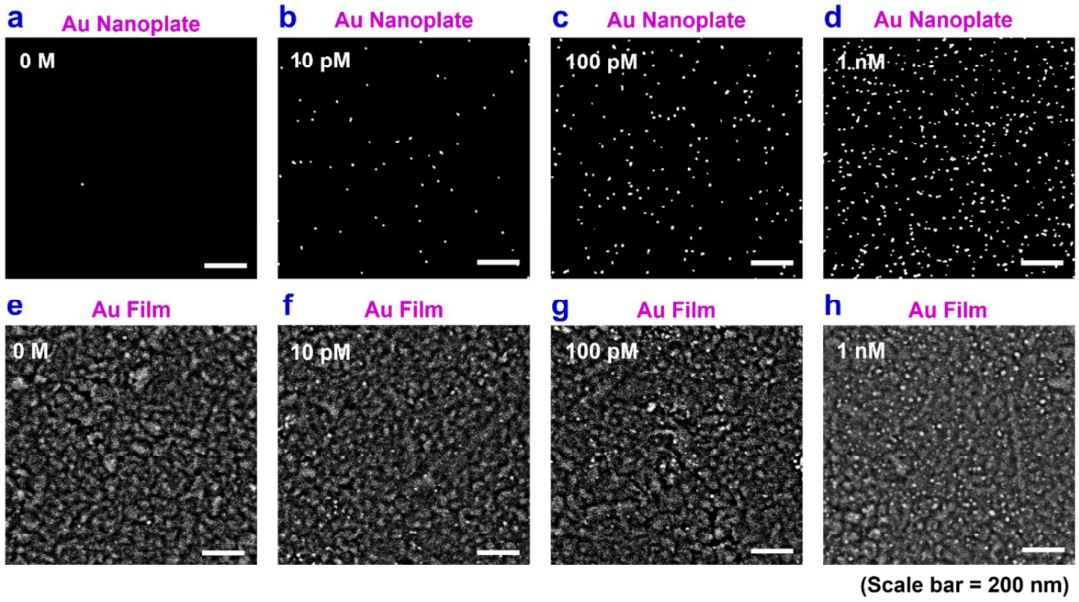

Figure S8. SEM images of Au NPs attached on (a-d) Au nanoplate and (e-h) Au film at various concentrations of avidin (0 M, 10 pM, 100 pM, 1 nM).